

WAVEFORM ANALYSIS TECHNIQUES IN AIRBORNE LASER SCANNING

W. Wagner^a, A. Roncat^a, T. Melzer^a, A. Ullrich^b

^a Christian Doppler Laboratory for Spatial Data from Laser Scanning and Remote Sensing, Institute of Photogrammetry and Remote Sensing, Vienna University of Technology, Gusshausstrasse 27-29, 1040 Wien, Austria
(ww, ar, tm)@ipf.tuwien.ac.at

^b Riegler Research GmbH, 3580 Horn, Austria - aullrich@riegler.co.at

KEY WORDS: LIDAR, Waveform, Analysis, Pulse detection, Decomposition, Deconvolution, Point cloud

ABSTRACT:

Small-footprint airborne laser scanners with waveform-digitising capabilities are becoming increasingly available. Waveform-digitising is particularly advantageous when the backscattered echo waveform is complex because it allows selecting processing algorithms adjusted to the task. In addition, waveform-digitising laser scanners depict the physical measurement process in its entire complexity. This opens the possibility to derive the backscatter cross section which is a measure of the electromagnetic energy intercepted and reradiated by objects. In this paper approaches for deriving the cross section along the laser ray path are discussed. For data storage and processing reasons a practical approach is to model the waveform as the sum of a number of echoes backscattered from individual scatterers. This approach involves estimating the number of echoes, finding a match between the modelled echoes and the measured waveform, and estimating the cross section using calibration targets. For estimating the number and position of echoes the Average Square Difference Function (ASDF) method, which is a discrete time delay estimation technique, is tested. The results show that ASDF is a promising approach which appears to be less affected by noise compared to more traditional echo detection methods.

1. INTRODUCTION

Airborne laser scanning (ALS) is an optical measurement technique for obtaining information about the Earth's surface such as the topography of the land surface, the vegetation cover and the seafloor elevation in shallow waters. This technique is also often referred to as LIDAR, which stands for *Light Detection And Ranging*. Most ALS instruments use pulse lasers, i.e. they send out short laser pulses in the visible and/or infrared part of the electromagnetic spectrum and measure some properties of the backscattered light to find range and/or other information of a distant target. While many of the first ALS systems provided only range information, ALS systems that digitise and record the complete echo waveform are becoming increasingly available.

Bathymetric lidar instruments designed for measuring depth of relatively shallow, coastal waters were the first full-waveform systems. These sensors transmit pulses at green wavelengths that penetrate several meters into the water depending on water clarity and turbidity. According to Wozencraft and Millar (2005) the maximum detectable depth of the seafloor is about 60 m. Scattering and spreading of the laser pulse at the air-water boundary, within the water column and the seafloor results in relatively complex echo waveforms (Tulldahl and Steinvall, 1999). Therefore, as Guenther et al. (2000) point out, it has not been possible to calculate all depths with high accuracy and reliability in real time during data acquisition. Precise depths are determined via post-flight processing of stored waveforms. More recently, NASA developed a small-footprint waveform-digitising bathymetric lidar that is also capable of mapping topography and vegetation (Wright and Brock, 2002). Nayegandhi et al. (2006) demonstrate the capability of this sensor for depicting the vertical structure of vegetation canopies.

Also the echo waveform from vegetated areas is in general rather complex, in particular when the laser footprint is large (Sun and Ranson, 2000). Therefore also large-footprint airborne and spaceborne lidar systems designed for mapping of vegetation capture the complete echo waveform in order to allow the retrieval of geophysical parameters in post-processing. One of the airborne systems is the Laser Vegetation Imaging Sensor (LVIS) that transmits 10 ns long infrared pulses at repetition rates up to 500 Hz (Blair et al., 1999). Depending on flight altitude the footprint diameter is 1-80 m. So far, no satellite lidar system designed for the primary purpose of global vegetation mapping is available. However, the Geoscience Laser Altimeter System (GLAS) on-board of the ICESat satellite has acquired waveform data not only over the ice sheets but also over land surfaces. This will allow testing the usefulness of large-footprint (66 m) satellite-based waveform measurements for characterising forest structure and biomass (Harding and Carabajal, 2005).

For topographic mapping a small laser footprint and a high point density are required to collect a high number of geometrically well defined terrain echoes. Various filters that classify the echoes into terrain and off-terrain echoes based on purely geometric criteria can be used to reconstruct the terrain surface (Sithole and Vosselman, 2004). Given that this approach has worked well for lidar systems with ranging capabilities only, the need for waveform digitising lidar systems has not been evident for this application. Also, the benefit of waveform data for emerging ALS applications like 3D city modelling (Vosselman et al., 2005) and forest mapping (Hollaus et al., 2006) was not clear even though some early studies demonstrated the rich information content of small-footprint waveform data over land surfaces (Lin, 1997). Nevertheless, the first commercial waveform-digitising laser scanner system started appearing in the market in 2004. Even though research

on small-footprint waveform data can still be considered to be only in its beginning, a number of benefits start to emerge:

- Jutzi and Stilla (2003) point out that recording the waveform is advantageous because algorithms can be adjusted to tasks, intermediate results are respected, and neighbourhood relations of pulses can be considered. For example, Wagner et al. (2004) show that depending on the observed target the range determined by different echo detection methods may differ by several decimetres for a laser footprint diameter of 1 m. Recording the waveform allows applying different detectors for different targets.
- Over forested areas the number of detected echoes can be significantly higher for waveform-recording ALS systems compared to first/last pulse systems (Persson et al., 2005; Reitberger et al., 2006)
- In addition to geometric information, waveform digitising ALS systems also provide a number of physical observables such as the echo width, the echo amplitude and the backscatter cross section (Wagner et al., 2006). This opens the possibility to classify the echo point cloud based on geometric and physical properties.
- The echo from vegetation is in general broader than the echo from the ground surface (Persson et al., 2005). Doneus and Briese (2006) demonstrated that it is possible to improve the quality of terrain models by removing wide echoes before the filtering process.
- The intensity of laser echoes, respectively the backscatter cross section, can be calibrated using portable brightness targets (Kaasalainen et al., 2005). This is important to enable the comparison of measurements taken by different sensors over different areas.
- In electrodynamics, scattering processes are described quantitatively by the cross section. The cross section is hence a fundamental quantity in radar and lidar remote sensing. Since it can be derived from calibrated waveform data, the gap between experimental results and electromagnetic theory could be bridged (Wagner et al., 2007).

In this paper waveform analysis techniques as applied to small-footprint ALS data acquired over land surfaces are discussed. An advanced method for estimating the number and position of echoes in small-footprint waveforms is investigated in more detail.

2. THEORY

2.1 Waveform Generation

The shape of the waveform is determined by a number of sensor parameters and the backscattering properties of the targets. Important sensor parameters are the shape of the laser pulse, the receiver impulse function and parameters describing the pulse spreading (Jutzi and Stilla, 2006). The target is described by the differential backscatter cross section $\sigma(t)$, whereas t represents the round-trip time from the sensor to the target and back. Essentially, the received power $P_r(t)$, i.e. the waveform, is the result of a convolution of the ALS system waveform $S(t)$ and the cross section $\sigma(t)$ (Wagner et al., 2006):

$$P_r(t) \propto S(t) * \sigma(t) \quad (1)$$

where the symbol $*$ represents the convolution operator. The system waveform $S(t)$ takes into account the form of the laser pulse and the effects of the receiver and other hardware components. For extended targets the convolution function given in Eq. (1) has to be expanded to account for beam spreading effects.

2.2 Backscatter Cross Section

As one is interested in measuring target characteristics, the principal quantity of interest in Eq. (1) is the differential backscatter cross section $\sigma(t)$, here also referred to cross section profile. It can be estimated from the measured waveform using deconvolution or decomposition techniques, each of which rests on a set of different assumptions about the real form of the cross section $\sigma(t)$.

Depending on the intended purpose, the cross section is treated as a continuous variable or as the sum of discrete values at different ranges. If treated as a continuous parameter the differential cross section can be represented in a three-dimension grid (voxel space). According to the orientation of the scanner relative to the 3D world frame, each ray (laser pulse) traces out a line in the world frame (Figure 1). Each voxel is assigned the corresponding value of the differential cross section. Such 3D representations could be the starting point for advanced modelling efforts, such as ray-tracing simulations within vegetation canopies (Sun and Ranson, 2000). A major disadvantage of such a representation is the required data volume.

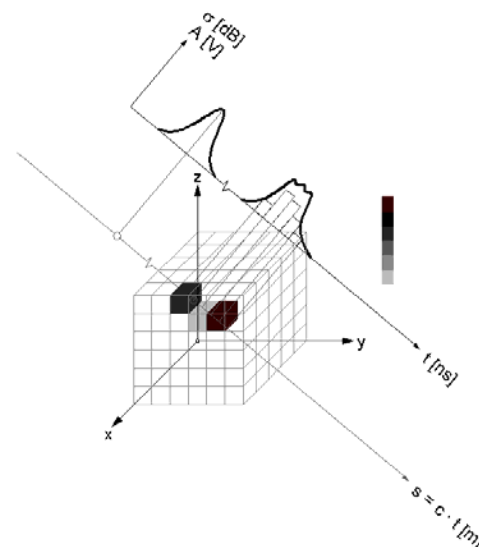


Figure 1. Voxel space representation of the cross section. The top half of the figure shows the emitted pulse (left) and the received echo (right), the lower half the embedding of the underlying cross section in a 3D voxel space.

For data storage and processing reasons a more practical approach is to model the waveform as the superposition of basis functions corresponding to the cross section of singular scatterers at different ranges (Wagner et al., 2006):

$$P_r(t) = \sum_{i=1}^N \frac{D_r^2}{4\pi R_i^4 \beta_i^2} \eta_{sys} \eta_{atm} S(t) * \sigma_i(t) \quad (2)$$

where N = number of targets
 D_r = receiver aperture diameter
 R_i = range from sensor to target i
 η_{sys} = system transmission factor
 η_{atm} = atmospheric transmission factor
 β_i = transmitter beamwidth
 σ_i = differential backscatter cross section of target i

Here, the waveform respectively cross section is represented by intermittent points irregularly distributed in 3D space (Figure 2). Neighbourhood relationships are not considered. An echo point is attributed a certain spatial dimension by adding the attribute “echo width”. This approach is currently the standard in ALS processing.

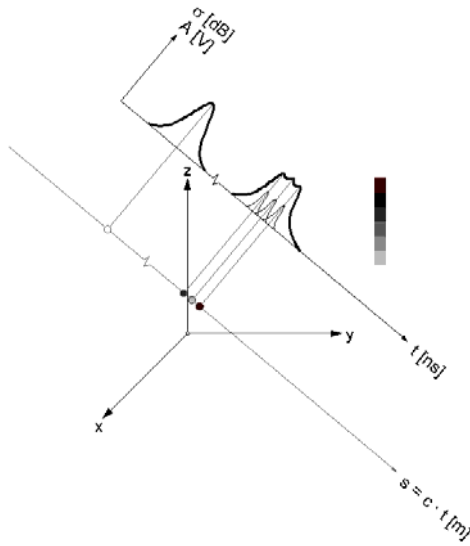


Figure 2. Discretisation of the ALS waveforms to obtain an irregularly distributed 3D point cloud. Here, the observed waveform is modelled explicitly as superposition of 3 Gaussian basis functions (targets).

2.3 Gaussian Decomposition

The decomposition of the waveform according to Eq. (2) becomes particularly simple, if both the individual cross sections and the emitted laser pulse can be described sufficiently well by Gaussian functions. In this case, the cross section can be computed in closed form using calibration targets (Wagner et al., 2006):

$$P_r(t) = \sum_{i=1}^N \hat{P}_i e^{-\frac{(t-t_i)^2}{2s_{p,i}^2}} \quad (3)$$

$$\sigma_i = C_{cal} R_i^4 \hat{P}_i s_{p,i} \quad (4)$$

where \hat{P}_i = amplitude of echo i
 $s_{p,i}$ = width of echo i
 t_i = round-trip time sensor to target i
 C_{cal} = calibration constant

Gaussian decomposition works by computing a nonlinear fit of the model Eq. (3) to the observed waveform. From the computed estimate (reconstruction), various target specific parameters such as echo width, intensity and position can be obtained. However, the number of targets as well as initial estimates for the distance of the targets have to be determined prior to the fit. This task is referred to as echo (pulse) detection.

Determining the number of echoes in ALS waveforms is not as simple as it may sound. Standard pulse detection methods such as *threshold*, *centre of gravity*, *maximum*, *zero crossing* of the second derivative, and *constant fraction* are discussed in Wagner et al. (2004). All these methods have their advantages and disadvantages. Problems occur when the waveforms have a complex shape and when the backscattered pulse is low compared to the noise level. In this case, advanced detection methods that minimise the influence of noise and account for non-ideal pulse forms should be sought. Thiel et al. (2005) tested a pulse correlation method and found almost no dependency on the signal to noise ratio. In our study we tested a time delay estimation technique as discussed in the next section.

3. ECHO DETECTION

For echo detection and time delay estimation, the *Average Square Difference Function* (ASDF) technique became relatively widespread during the last 15 years. Given two equidistantly sampled discrete time series, $x_1(t)$ and $x_2(t)$, the response value R of the ASDF is defined as (Jacovitti and Scarano, 1993):

$$R_{ASDF}(\tau) = \sum_{k=1}^n [x_1(kT) - x_2(kT + \tau)]^2 \quad (5)$$

where T is the sampling interval and $(n-1)T$ the estimation window length. Figure 3 (bottom) shows a typical example of $R_{ASDF}(\tau)$. As one can see, this function is closely related to the well-known direct cross-correlation function but has some computational advantages (Jacovitti and Scarano, 1993). In the case of full-waveform analysis, the reference pulse $x_1(t)$ can be of any shape required by the respective task, e.g.

- the emitted laser pulse itself (see Figure 3, top)
- a Gaussian Pulse (see Figure 4) or
- a mean reference system waveform (see Figure 4) derived from a set of original laser pulses.

The time delay estimator Δt of a tentative echo is the value of τ corresponding to the minimum of $R_{ASDF}(\tau)$. In full-waveform laser scanning, one has to expect multiple echoes of a single laser pulse. Therefore, not only the global minimum, but also the local minima have to be taken into account. Tentative echoes are located between local maxima (depicted with black circles in Figure 5). Due to the fact that only positive values of R_{ASDF} appear and due to zero-padding outside the time window of x_2 , the values of R_{ASDF} at the margins of its time window are always considered as local maxima (Figure 5). To distinguish real echoes from background noise, the detected minima must be separated from the neighbouring minima by a minimum distance ΔR_{min} . For our calculations we choose:

$$\Delta R_{min} = 0.3(\max(R_{ASDF}(\tau)) - \min(R_{ASDF}(\tau))) \quad (6)$$

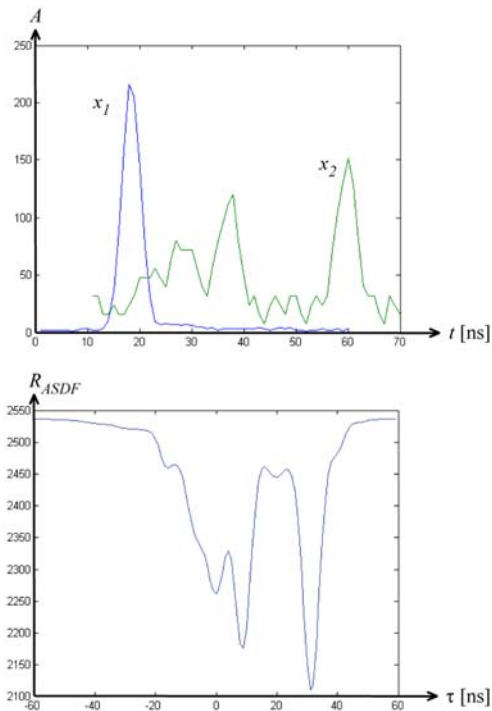


Figure 3. Top: Two discrete time series $x_1(t)$ (blue line) and $x_2(t)$ (green line) representing the system waveform and the backscattered waveform. Bottom: ASDF of these two time series.

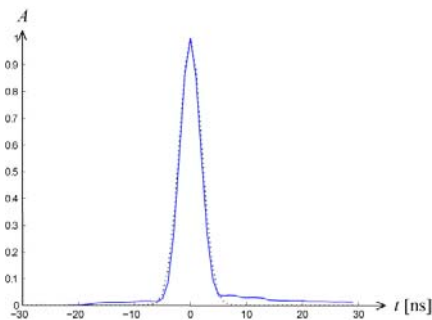


Figure 4. Mean reference pulse of the Riegl LMS-Q560 (blue solid line) and Gaussian pulse (black dotted line).

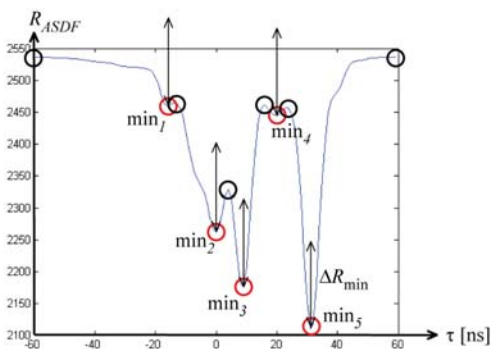


Figure 5. Principle of echo detection using ASDF.

Until now, the time delay of the detected echoes is only coarsely determined in the dimension of the sampling interval. According to Jacovitti and Scarano (1993), parabola fitting can be used for fine delay estimation. The peak of this parabola is located at

$$\Delta t_{fine} = -\frac{T}{2} \frac{R_{ASDF}(\Delta t + T) - R_{ASDF}(\Delta t - T)}{R_{ASDF}(\Delta t + T) - 2R_{ASDF}(\Delta t) + R_{ASDF}(\Delta t - T)} + \Delta t. \quad (7)$$

4. EXPERIMENTS

In this section, we present the results of two simple pulse detection and estimation experiments.

4.1 Data Sets

The data used in this study consist of two samples from the 2005 flight campaign over the Schönbrunn area of Vienna using the Riegl LMS-Q560 full-waveform laser scanner which uses a digitising interval of 1 ns. This campaign consisted of 14 flight strips (side overlap 60%) with an altitude of 500 m above ground and an average point density of 4 points per square metre within the strip. The data were acquired on April 5th, 2005 before the greening-up of the vegetation. Each sample contains the waveforms of 10,000 consecutive laser pulses and was taken from an area with rather dense vegetation (see Figure 6).

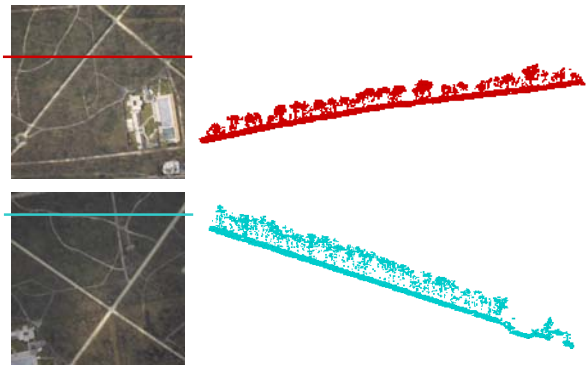


Figure 6. Aerial and perspective views of the sample areas. Top: Sample 1 (strip 2), bottom: Sample 2 (strip 5).

4.2 Results

In the first experiment, the number of echoes obtained with the max-detection method and two ASDF-based methods were compared. Max-detection considers those points as maxima whose intensity exceeds the respective intensities of its immediate neighbours. It is one of our standard pulse detection methods used in Gaussian Decomposition. The first ASDF-based technique uses a Gaussian Pulse with $s_p = 2$ ns as reference pulse (x_1 in Eq. (3)) whereas the second ASDF-based technique used the average of all emitted pulses of the respective sample as reference pulse. The results of this comparison are given in Table 1.

Method	# detected echoes (%)				
	1	2	3	4	>= 5
Max-Detection	58,08	32,20	7,73	1,08	0,09
ASDF (Gaussian Pulse)	66,23	21,09	9,22	1,81	0,18
ASDF (Mean Reference Pulse)	65,89	20,65	9,74	2,01	0,24

Method	# detected echoes (%)				
	1	2	3	4	>= 5
Max-Detection	51,54	35,23	10,86	1,67	0,27
ASDF (Gaussian Pulse)	60,96	24,24	11,48	2,47	0,24
ASDF (Mean Reference Pulse)	60,64	23,63	12,15	2,70	0,27

Table 1. Number of Echoes computed with Max-Detection vs. ASDF-based Pulse Detection. Top: Sample 1 (Strip 2), bottom: Sample 2 (Strip 5).

From Table 1 one can learn that the used reference pulse of the ASDF-based techniques does not influence the results of pulse detection significantly. However, it is not clear if this is mainly a consequence of the scanner's recording system. Comparing max-detection with the ASDF-based methods, one can see that the latter are more likely to detect single echoes than max-detection. It appears that ASDF is less sensitive to laser ringing effects, which may be pronounced particularly after strong echoes (Nordin, 2006). On the other hand, Table 1 shows that it is also more likely to detect three and more echoes with an ASDF-based technique than with max-detection.

In the second experiment, the echo estimation of the three different methods (Gaussian Decomposition and the two ASDF-based approaches mentioned above) was compared. Two echoes computed with different estimation methods were treated as identical (one and the same) if their respective delays Δt did not differ more than the sampling interval of 1 ns (see Table 2).

Comparison	Identical echoes (%)		Median of difference [ns]		RMS of difference [ns]	
	Sample 1	Sample 2	Sample 1	Sample 2	Sample 1	Sample 2
Gaussian Decomposition / ASDF (Gauss.Pulse)	86,7	86,4	-0,0004	-0,0004	0,12	0,13
Gaussian Decomposition / ASDF (Mean Ref. Pulse)	86,9	86,8	0,0002	-7E-05	0,12	0,13
ASDF (Mean Ref. Pulse) / ASDF (Gauss.Pulse)	98,7	98,7	-0,0008	-0,001	0,05	0,05

Table 2. Comparison of Echo Estimation

The results of Table 2 show that in most cases (more than 85 %), classical pulse detection methods and ASDF-based approaches yield identical pulses. Also here, the two ASDF-variants show nearly identical results. Furthermore, it is given empirical evidence that in most cases echo estimation with Gaussian decomposition and with parabola fitting of the ASDF lead to comparable results since the medians of difference are very close to 0 and the standard deviations of difference are not greater than 0.15 ns. In metric dimensions, this would conform to 2.25 cm in the direction of the laser pulse which is a very low value in comparison to the ranges appearing in ALS.

5. CONCLUSIONS

The experiments presented in this paper give empirical evidence that both pulse detection and pulse estimation using the Average Square Difference Function (ASDF) method is a

promising approach. To a high percentage, the results of ASDF-based techniques coincide with those achieved using standard methods. In these cases, it would not be necessary to determine the exact position of the echoes with non-linear fitting methods but could be done prior to Gaussian decomposition using the ASDF technique. This could accelerate the calculations, what is important given the increasingly large data volumes that novel laser scanner systems deliver. The remaining cases, where classical pulse detection methods and ASDF-based techniques do not coincide, need to be treated in more detail and are subject of further research.

6. REFERENCES

Blair, J. B., Rabine, D. L., and Hofton, M. A., 1999. The Laser Vegetation Imaging Sensor: a medium-altitude, digitisation-only, airborne laser altimeter for mapping vegetation and topography. *ISPRS Journal of Photogrammetry and Remote Sensing*, 54, pp. 115-122.

Doneus, M. and Briese, C., 2006. Digital terrain modelling for archaeological interpretation within forested areas using full-waveform laserscanning. In: M. Ioannides, D. Arnold, F. Niccolucci and K. Mania (Editors), *The 7th International Symposium on Virtual Reality, Archaeology and Cultural Heritage VAST (2006)*, in press.

Guenther, G.C., Cunningham, G.C., LaRocque, P.E., and Reid, D.J., 2000. Meeting the accuracy challenge in airborne lidar bathymetry. In: *Proceedings of the EARSeL-SIG-Workshop LIDAR*, Dresden, Germany, June 16-17, European Association of Remote Sensing Laboratories, 23 p.

Harding, D.J., and Carabajal, C.C., 2005. ICESat waveform measurements of within-footprint topographic relief and vegetation vertical structure. *Geophysical Research Letters*, 32, L21S10, pp. 1-4.

Hollaus, M., Wagner, W., Eberhöfer, C., and Karel, W., 2006. Accuracy of large-scale canopy heights derived from LiDAR data under operational constraints in a complex alpine environment. *ISPRS Journal of Photogrammetry and Remote Sensing*, 60(5), pp. 323-338.

Jacovitti, G., Scarano, G., 1993. Discrete Time Techniques for Time Delay Estimation. *IEEE Transactions on Signal Processing*, 41(2), pp. 525-533.

Jutzi, B., and Stilla, U., 2003. Laser pulse analysis for reconstruction and classification of urban objects. In: *International Archives of Photogrammetry and Remote Sensing*, Munich, Germany, 17-19. Sept., Vol. 34, Part 3/W8, pp. 151-156.

Jutzi, B., and Stilla, U., 2006. Range determination with waveform recording laser systems using a Wiener filter. *ISPRS Journal of Photogrammetry and Remote Sensing*, 61, pp. 95-107.

Kaasalainen, S., Ahokas, E., Hyypä, J., and Suomalainen, J., 2005. Study of surface brightness from backscattered laser intensity: Calibration of laser data. *IEEE Geoscience and Remote Sensing Letters*, 2(3), pp. 255-259.

- Lin, C.S., 1997. Waveform sampling lidar applications in complex terrain. *International Journal of Remote Sensing*, 18(10), pp. 2087-2104.
- Nayegandhi, A., Brock, J.C., Wright, C.W., and O'Connell, M.J., 2006. Evaluating a small footprint, waveform-resolving lidar over coastal vegetation communities. *Photogrammetric Engineering & Remote Sensing*, 72(12), pp. 1407-1417.
- Nordin, L., 2006. Analysis of waveform data from airborne laser scanner systems. Master Thesis, Luleå University of Technology.
- Persson, Å., Söderman, U., Töpel, J., and Ahlberg, S., 2005. Visualization and analysis of full-waveform airborne laser scanner data. In: *International Archives of Photogrammetry and Remote Sensing*, Vol. 36, Part 3/W19, pp. 103-108.
- Reitberger, J., Krzystek, P., and Heurich, M., 2006. Full-waveform analysis of small footprint airborne laser scanning data in the Bavarian forest national park for tree species classification. In: *Proceedings of the International Workshop on 3D Remote Sensing in Forestry*, Vienna, Austria, 14-15. Feb., pp. 218-227.
- Sithole, G., and Vosselman, G., 2004. Experimental comparison of filter algorithms for bare-Earth extraction from airborne laser scanning point clouds. *ISPRS Journal of Photogrammetry & Remote Sensing*, 59, pp. 85-101.
- Sun, G., and Ranson, K.J., 2000. Modeling lidar returns from forest canopies. *IEEE Transactions on Geoscience and Remote Sensing*, 38(6), pp. 2617-2626.
- Tiehl, K.-H., Wehr, A., and Hug, C., 2005. A new algorithm for processing fullwave laser scanner data. In: Proceedings of EARSEL Workshop "Use the third dimension for remote sensing purposed", Porto, Portugal.
- Tulldahl, H.M., and Steinvall, K.O., 1999. Analytical waveform generation from small objects in lidar bathymetry. *Applied Optics*, 38(6), pp. 1021-1039.
- Vosselman, G., Kessels, P., and Gorte, B., 2005. The utilization of airborne laser scanning for mapping. *International Journal of Applied Earth Observation and Geoinformation*, 6, pp. 177-186.
- Wagner, W., Ullrich, A., Melzer, T., Briese, C., and Kraus, K., 2004. From single-pulse to full-waveform airborne laser scanners: Potential and practical challenges. In: *International Archives of Photogrammetry and Remote Sensing*, XXth ISPRS Congress, Istanbul, Turkey, 12-23 July 2004, Vol. XXXV, Part B3, pp. 201-206.
- Wagner, W., Ullrich, A., Ducic, V., Melzer, T., and Studnicka, N., 2006. Gaussian decomposition and calibration of a novel small-footprint full-waveform digitising airborne laser scanner. *ISPRS Journal of Photogrammetry and Remote Sensing*, 60(2), pp. 100-112.
- Wagner, W., Hollaus, M., Briese, C., and Ducic, V., 2007. 3D vegetation mapping using small-footprint full-waveform airborne laser scanners. *International Journal of Remote Sensing*, in press.
- Wright, C.W., and Brock, J.C., 2002. EAARL: A Lidar for mapping shallow coral reefs and other coastal environments. In: *Proceedings of the Seventh International Conference on Remote Sensing for Marine and Coastal Environments*, Miami, Florida, unpaginated CDROM.
- Wozencraft, J., and Millar, D., 2005. Airborne lidar and integrated technologies for coastal mapping and nautical charting. *Marine Technology Society Journal*, 39(3), pp. 27-35.

7. ACKNOWLEDGEMENTS

We would like to thank the Schloß Schönbrunn Kultur- und Betriebsges.m.b.H for their support of the data acquisition campaign.